PFC/JA-85-6

Generalized Nonlinear Harmonic Gyrotron Theory

B.G.Danly and R.J.Temkin

Plasma Fusion Center
Massachusetts Institute of Technology
Cambridge, MA 02139

April 1985

This work was supported by the U.S. Department of Energy Contract No. DE-AC02-78ET51013.

Generalized Nonlinear Harmonic Gyrotron Theory

B.G.Danly and R.J.Temkin

Plasma Fusion Center
Massachusetts Institute of Technology
Cambridge, MA 02139

April, 1985

Abstract

The nonlinear efficiency for a gyrotron oscillator operating at harmonics of the cyclotron frequency has been calculated and is presented as a function of generalized parameters for the second through fifth harmonics. The numerical results are valid for a wide range of operating conditions, including voltage, current, beam radius, cavity dimensions, and operating mode. Relatively high efficiencies are found even at high harmonics; the maximum transverse efficiencies for harmonics 2,3,4, and 5 are 0.72,0.57,0.45, and 0.36, respectively. The calculation of the efficiency in terms of generalized parameters allows the straightforward design and optimization of harmonic gyrotrons. The influence of the axial profile of the rf field in the gyrotron cavity on the efficiency is also investigated. Improved efficiency can be achieved with asymmetric field profiles. The implications of these results for the generation of millimeter and submillimeter wave radiation by harmonic emission are discussed.

PACS 52.75.Ms, 85.10.Ka

I. INTRODUCTION

The gyrotron or electron cyclotron maser is one of the most promising sources for the generation of high power radiation in the microwave to submillimeter region of the spectrum [1-4]. Among its many important applications include the RF heating of fusion plasmas [5-7], plasma diagnostics [8,9], and radar.

Gyrotrons operate in circular TE modes near cutoff, that is $\omega/c = k = (k_\perp^2 + k_\parallel^2)^{1/2}$ with $k_\perp \gg k_\parallel$, where $k_\perp$ and $k_\parallel$ are the transverse and axial wavenumbers of the waveguide modes. In this case, we may take $\omega/c = k \approx k_\perp = \nu_{mp}/a$ for TE modes, where a is the cavity radius and ν_{mp} is the p^{th} zero of $J'_m(x)$. The combination of this condition and the cyclotron resonance condition, $\omega \approx n\omega_c$, determine the oscillation mode of a gyrotron. Here $\omega_c = eB/mc\gamma$ is the relativistic electron cyclotron frequency, n is the harmonic number,m and e are the relativistic electron rest mass and charge, and $\gamma = (1-\beta^2)^{-1/2}$ with $\beta = v/c$. The gyrotron interaction results from a phase bunching of electrons by an RF field due to the energy dependence of their cyclotron frequency.

With the growing demand for sources in the millimeter and submillimeter regions of the spectrum, increasing the gyrotron operating frequency becomes of primary importance. Gyrotrons are usually operated at the fundamental of the cyclotron frequency, $\omega \approx \omega_c$. Because the available magnetic field limits the maximum frequency that can be obtained, gyrotron operation at the fundamental is limited to lower frequencies. Operation at the second ($\omega \approx 2\omega_c$) or higher harmonics ($\omega \approx n\omega_c, n > 2$) might prove advantageous for several reasons. The magnetic field required to produce radiation at a given frequency is reduced by a factor of n for operation at the n^{th} harmonic. Consequently, much higher frequencies can be produced with modest magnetic fields. Alternatively, even for microwave and millimeter wave frequencies, operation at a harmonic allows the use of compact, less

costly magnets. It appears feasible that millimeter wave radiation could be generated by a harmonic gyrotron operating with permanent magnets.

During the past several years, impressive results have been obtained with gyrotrons designed for operation at harmonics of the cyclotron frequency. Zaytsev *et al.*[10] have reported the $2\omega_c$ generation of 7 kW at 154 GHz in pulsed operation and the $2\omega_c$ generation of 2.4 kW at 157 GHz and 1.5 kW at 326 GHz in CW operation. Several harmonic experiments have been carried out in the U.S. during the past decade[3,11,12], including the generation of 25 kW at 241 GHz in pulsed operation[13]. Guo *et al.* have produced 30 kW at 37 GHz[14], and Boulanger *et al.* have reported the generation of 30 kW at 70 GHz[15], both by second harmonic operation.

In the theoretical area, several authors have derived the linear theory of a harmonic gyrotron. Chu has presented a detailed treatment of a harmonic gyrotron in which the beam-wave coupling coefficient and beam energy gain function are derived.[16] Uhm *et al.* have presented a linear stability analysis for the cyclotron maser instability.[17] In several cases, nonlinear efficiency calculations for $2\omega_c$ operation on a specific cavity mode and under a specific set of operating conditions have also been carried out. Nusinovich and Erm have carried out a calculation of gyrotron efficiency for ω_c and $2\omega_c$ operation which is generally applicable to any cavity mode and a wide range of operating conditions[18]. The formalism employed here has been used by other authors.[18,20] We present here numerical results for a generalized nonlinear theory for gyrotrons operating on the first through fifth harmonics. These results are presented in terms of general normalized parameters and are thus applicable to many operating conditions.

This paper is organized as follows. The theory is reviewed in section II. The results for the nonlinear efficiency for the fundamental and the second through fifth harmonics of

the cyclotron frequency are presented in section III. Application of these results to the case of a quasioptical gyrotron is also discussed. The implications of the results are discussed in section IV, and the conclusions are presented in section V.

II. THEORY

The generalized nonlinear theory for a harmonic gyrotron oscillator can be developed in the form of generalized pendulum equations.[2,18–20] For an electron moving in combined electric and magnetic fields, the equations of motion are

$$\frac{d\mathcal{E}}{dt} = -e\mathbf{v}\cdot\mathbf{E} \tag{1}$$

$$\frac{d\mathbf{p}}{dt} = -e\mathbf{E} - \frac{e}{c}\mathbf{v}\times\mathbf{B} \tag{2}$$

where $\mathcal{E} = \gamma m_e c^2$ is the electron energy, $\gamma = (1-\beta_\perp^2-\beta_\parallel^2)^{-1/2}$ and $|\mathbf{p}| = \gamma\beta m_e c$ is the electron momentum. For a high Q gyrotron oscillator we specify the electromagnetic field structure in the cavity to be axially fixed, but we allow it to rotate in the azimuthal direction. The assumption of an axially fixed field structure is allowed provided the source term in Maxwell's equations is negligible; the electric field $\mathbf{E}$ is then that of a TE cavity mode. This assumption is not unrealistic for a harmonic gyrotron in which the diffractive Q (Q_D) is much higher than the minimum diffractive Q.[4,10] The effect of the rf magnetic field on the electron motion is negligible provided the phase velocity of the rf field is much greater than the speed of light, as is the case for a wave near cutoff.[20,21] The magnetic field is taken to be the axial static guide field $\mathbf{B} = B_0\mathbf{z}$, as shown in Fig.1.

The equation for the energy of a single electron can be written in terms of a relative energy variable $\mathrm{w} = 1 - \gamma/\gamma_0$ and a normalized axial position $Z = \omega z/\beta_{\parallel 0}c$ as

$$\frac{d\mathrm{w}}{dZ} = \frac{e}{(m_e c)^2\omega}\frac{\beta_{\parallel 0}}{\gamma_0\gamma\beta_\parallel}\,\mathbf{p}\cdot\mathbf{E} \tag{3}$$

Here $\beta_{\parallel 0}$ and γ_0 are the values of $\beta_\parallel$ and γ at the entrance to the cavity. A subscript zero indicates that the value of the variable is to be taken at the entrance to the interaction region. In complex notation, we write $\mathbf{p} = p_x + ip_y = p_+ = |p_+|e^{i\alpha}$, where α is defined in

Fig.1, and $\mathbf{E} = E_x + iE_y = E_+ = |E_+|e^{i(\omega t+\psi)}$. Then equation (3) can be expressed as

$$\frac{dw}{dZ} = \frac{e}{(m_e c)^2 \omega} \frac{\beta_{\|0}}{\gamma_0 \gamma \beta_{\|}} \text{Re}\,(p_+^* E_+)\,. \tag{4}$$

The equation for the phase of the electron can be derived from eqn.(2);

$$\frac{d\alpha}{dZ} = \frac{\beta_{\|0}\omega_c}{\beta_{\|}\omega} - \frac{e\beta_{\|0}}{\omega\beta_{\|}|p_+|} \text{Im}\,(p_+^* E_+)\,, \tag{5}$$

where $\omega_c = eB_0/m_e c\gamma$.

The electric field for a TE_{mp} mode near cutoff in a circular cross section cavity is written as

$$\mathbf{E} = (E_R \hat{R} + E_{\phi_0}\hat{\phi}_0)\, e^{i(\omega t+\psi)},$$

$$E_R = i\frac{m}{k_\perp R} E_0\, f(z)\, J_m(k_\perp R)\, e^{-im\phi_0},$$

$$E_{\phi_0} = E_0\, f(z)\, J'_m(k_\perp R)\, e^{-im\phi_0},$$

where (R, ϕ_0) are coordinates in the coordinate system with origin at the center of the cavity; $k_\perp = \nu_{mp}/a$ where ν_{mp} is the p^{th} nonvanishing zero of $J'_m(x)$, and a is the cavity radius. The field used here is that of a rotating mode. E_0 is the field amplitude, and $f(z)$ is the axial field distribution, the amplitude of which is normalized to unity. Using Graf's formula for Bessel functions, the electric field can be reexpressed as a series in a coordinate system with origin at the electron gyrocenter.[22] The component of the rf field synchronous with the electron for n^{th} order cyclotron resonance ($\omega \approx n\omega_c$) can then be written as

$$\mathbf{E} = (E_{rn}\hat{r} + E_{\phi n}\hat{\phi})\, e^{i(\omega t+\psi)},$$

$$E_{rn} = i\frac{n}{k_\perp r} E_0\, f(z)\, J_{m\pm n}(k_\perp R_e)\, J_n(k_\perp r)\, e^{-im\phi_0}\, e^{-in(\phi-\phi_0)},$$

$$E_{\phi n} = E_0\, f(z)\, J_{m\pm n}(k_\perp R_e)\, J'_n(k_\perp r)\, e^{-im\phi_0}\, e^{-in(\phi-\phi_0)}.$$

In complex notation, the electric field of a TE_{mp} cavity mode can then be written as

$$E_- = -E_r \sin(\theta + \psi - (m-n)\phi_0)\, e^{i\phi} + E_\phi \cos(\theta + \psi - (m-n)\phi_0)\, ie^{i\phi}$$

where E_r and E_ϕ are defined by $E_r = |E_{rn}|$ and $E_\phi = |E_{\phi n}|$. The slow-time scale phase variable $\theta = \omega t - n\phi$ has been introduced; the electron phase ϕ is related to α by $\alpha = \phi + \pi/2$. Evaluation of the real and imaginary parts of $E_- e^{-i\alpha}$ in equations (4) and (5) leads to the equations of motion

$$\frac{d\mathrm{w}}{dZ} = \frac{e}{\gamma_0 m_e c\omega} p'_\perp E_\phi \cos(\theta + \psi - (m-n)\phi_0) \tag{6}$$

$$\frac{d\theta}{dZ} = \delta_0 - \mathrm{w} - \frac{ne}{\gamma_0 m_e c\omega} \frac{(1-\mathrm{w})}{p'_\perp} E_r \sin(\theta - \psi - (m-n)\phi_0) \tag{7}$$

where

$$p'_\perp = \frac{|p_+|}{\gamma_0 m_e c} = (\beta^2_{\perp 0} - 2\mathrm{w} + \mathrm{w}^2)^{\frac{1}{2}},$$

and $\delta_0 = 1 - n\omega_{c0}/\omega$, where $\omega_{c0} = eB/m_e c\gamma_0$, is the magnetic field detuning parameter. For gyromonotrons, the electron beam at the entrance to the cavity has no bunching, and, consequently, the value of ψ at the entrance to the cavity is arbitrary. In general ψ can depend on Z; we assume ψ is constant throughout the interaction region. Choosing $\psi - (m-n)\phi_0 = -\frac{\pi}{2}$, and writing $\omega \approx n\omega_{c0}$, the above equations reduce to

$$\frac{d\mathrm{w}}{dZ} = \frac{E_\phi}{nB_0} p'_\perp \sin\theta \tag{8}$$

$$\frac{d\theta}{dZ} = \delta_0 - \mathrm{w} - \frac{E_r}{B_0} \frac{(1-\mathrm{w})}{p'_\perp} \cos\theta \tag{9}$$

The inertial bunching is a result of the action of the azimuthal electric field E_ϕ; it is directly responsible for the variation of electron energy (equation (8)). The force bunching results from the radial electric field E_r, and contributes through equation (9) to the phase bunching. In most gyrotrons the dominant contribution to the phase bunching is from the inertial bunching term. Because the Larmor orbit depends on the electron energy, the argument of the Bessel functions in the expressions for E_r and E_ϕ can be expressed in terms of the energy variable;

$$k_\perp r \approx n\frac{\gamma\beta_\perp}{\gamma_0} = n\beta_{\perp 0}\left(1 - \frac{1}{\beta^2_{\perp 0}}(2\mathrm{w} - \mathrm{w}^2)\right)^{\frac{1}{2}} = np'_\perp.$$

At this point it is useful to redefine the dependent and independent variables according to

$$u \equiv \frac{2}{\beta_{\perp 0}^2} \mathrm{w} = \frac{2}{\beta_{\perp 0}^2}\left(1 - \frac{\gamma}{\gamma_0}\right)$$
$$\varsigma \equiv \frac{\beta_{\perp 0}^2}{2} Z = \pi \frac{\beta_{\perp 0}^2}{\beta_{\parallel 0}} \frac{z}{\lambda}.$$

The normalized interaction length is then defined as

$$\mu \equiv \pi \frac{\beta_{\perp 0}^2}{\beta_{\parallel 0}} \frac{L}{\lambda}.$$

Then equations (8) and (9) can be written as

$$\frac{du}{d\varsigma} = 2\left(\frac{2^n n!}{n^n \beta_{\perp 0}^{n-1}}\right) F f(\varsigma) \frac{p'_\perp}{\beta_{\perp 0}} J'_n(n p'_\perp) \sin\theta \tag{10}$$

$$\frac{d\theta}{d\varsigma} = \Delta - u - n\left(\frac{2^n n!}{n^n \beta_{\perp 0}^{n-1}}\right) F f(\varsigma) \frac{\beta_{\perp 0}(1 - \beta_{\perp 0}^2 u/2)}{p'^2_\perp} J_n(n p'_\perp) \cos\theta, \tag{11}$$

where the normalized field amplitude F is defined by

$$F \equiv \frac{E_0}{B_0} \beta_{\perp 0}^{n-4} \left(\frac{n^{n-1}}{n! 2^{n-1}}\right) J_{m \pm n}(k_\perp R_e)$$

and the detuning parameter $\Delta \equiv 2\delta_0/\beta_{\perp 0}^2$. The plus and minus signs in the Bessel function subscript correspond to the two possible rotations of the rf field. The initial conditions are $\theta = \theta_0 \in [0, 2\pi)$ and $u = 0$. The efficiency is given by

$$\eta \equiv \frac{\gamma_0 - \gamma}{\gamma_0 - 1} = \frac{\beta_{\perp 0}^2}{2(1 - \gamma_0^{-1})} \eta_\perp.$$

where

$$\eta_\perp = \langle u(\varsigma_{out}) \rangle_{\theta_0}$$

is the transverse efficiency. The brackets denote an average over initial phase. Equations (10) and (11) are exact for a gyrotron interaction ($k_\parallel c/\omega \approx 0$); only the asynchronous

components of the rf field have been neglected (slow time scale approximation). As apparent from these equations, the transverse or perpendicular efficiency depends only upon four normalized parameters, F, μ, Δ, and $\beta_{\perp 0}$.

Under certain conditions, the equations of motion can be simplified further, and the parameters describing the problem can be reduced to F, μ, and Δ. When the electron beam is weakly relativistic, and the condition

$$\frac{n\beta_{\perp 0}^2}{2} \ll 1 \tag{12}$$

is satisfied, then $p'_\perp$ may be approximated by [20]

$$p'_\perp \approx \left(\beta_{\perp 0}^2 - 2\mathrm{w}\right)^{\frac{1}{2}} = \beta_{\perp 0}\left(1-u\right)^{\frac{1}{2}}.$$

Furthermore, provided the condition in equation (12) is satisfied, the small argument expansion of the Bessel functions in equations (10) and (11) can be made. Equations (10) and (11) then simplify to

$$\frac{du}{d\zeta} = 2F\, f(\zeta)\, (1-u)^{\frac{n}{2}}\, \sin\theta \tag{13}$$

$$\frac{d\theta}{d\zeta} = \Delta - u - n\,F\, f(\zeta)\, (1-u)^{\frac{n}{2}-1}\, \cos\theta \tag{14}$$

In this case the perpendicular efficiency depends only on three parameters (F, μ,and Δ). The efficiency is generally optimized with respect to the magnetic field parameter Δ; the optimum value of Δ is denoted Δ_{opt}.

The field amplitude F is related to the beam current by an energy balance equation. The total cavity Q, Q_T, is related to the total stored energy U and the power dissipated P by $Q_T = \omega U/P$. The power dissipated is written as

$$P = \eta\, I_A\, V = \frac{mc^2}{e}\,\frac{\gamma_0\beta_{\perp 0}^2}{2}\,\eta_\perp\, I_A,$$

where I_A is the beam current. Evaluation of the stored energy requires a choice of the axial field profile. Most actual axial field profiles are closely approximated by a Gaussian. We assume the axial field profile is given by

$$f(z) = e^{-(k_{\|}z)^2} \quad \text{or} \quad f(\varsigma) = e^{-(2\varsigma/\mu)^2}, \tag{15}$$

where $k_{\|} = 2/L$ defines the effective cavity length L. The energy balance equation can then be written as

$$F^2 = \eta_{\perp} I, \tag{16}$$

where a normalized current parameter I has been introduced. I is defined by

$$I = 0.238 \times 10^{-3} \frac{Q_T I_A}{\gamma_0} \beta_{\perp 0}^{2(n-3)} \left(\frac{\lambda}{L}\right) \left(\frac{n^n}{2^n n!}\right)^2 \frac{J_{m\pm n}^2 (k_{\perp} R_e)}{\left(\nu_{mp}^2 - m^2\right) J_m^2 (\nu_{mp})},$$

where I_A is the beam current in amps. Once the optimized efficiency is calculated for specific values of F and μ, the beam current necessary to achieve that value of F and $\eta_{\perp}$ is given by equation (16).

Because the optimized efficiency can be written as a function of only two parameters, $\eta_{\perp} = \eta_{\perp}(F, \mu)$, the results of a numerical integration of equations (13) and (14) can be conveniently presented in the form of a single contour plot of the efficiency $\eta_{\perp}$ in F-μ space. The corresponding contour plot of efficiency as a function of the beam current parameter I and cavity length μ can be obtained by application of eqn.(16) to the data in the $\eta_{\perp}(F, \mu)$ contour plot. The $\eta_{\perp}(I, \mu)$ contour plot is most useful for determination of theoretical efficiencies for given values of beam current. The $\eta_{\perp}(F, \mu)$ contour plot is most useful for the optimization of gyrotron design, because the relevant design constraints such as wall loading, beam voltage depression, and beam thickness effects, can be expressed in terms of the F and μ parameters in a straightforward manner.[23]

III. RESULTS

The efficiency of gyrotron operation at the fundamental of the cyclotron frequency and at the second through the fifth harmonics has been calculated. The equations describing the weakly relativistic gyrotron (eqns.(13) and (14)) were integrated numerically using a fourth order Runge-Kutta algorithm for the Gaussian axial field profile given by eqn.(15). The limits chosen for the integration over the axial field profile were $\varsigma = -\sqrt{3}\mu/2$ to $+\sqrt{3}\mu/2$, which correspond to the e^{-3} power points of the axial rf field; they are a good approximation to actual tapered gyrotron resonators.[4,19] The ensemble average over initial phase was carried out by integrating 32 different particles, evenly distributed in phase, and averaging the resulting single particle efficiencies. Optimization of the efficiency with respect to the magnetic field parameter (Δ) was also performed. The optimized efficiency was calculated for a large number (800-1600) of different values of F and μ; the $\eta_\perp(F,\mu)$ isoefficiency contour plots are generated from this data.

Results for the optimized efficiency at the fundamental cyclotron resonance are shown in Figs. 2 and 3. The perpendicular efficiency (solid lines) as a function of normalized rf field amplitude and cavity length (F-μ contour plot) is shown in Fig. 2; the efficiency as a function of the normalized beam current and cavity length (I-μ contour plot) is shown in Fig. 3. Contours of the optimum magnetic field detuning (Δ_{opt}) are shown as dashed lines in Fig. 2.

The starting current of a gyrotron operating at the n^{th} harmonic is given in terms of the normalized parameter I by [24]

$$I_{ST}(\Delta,\mu) = \frac{4}{\pi\mu^2}\,\frac{e^{2x^2}}{\mu x - n}, \tag{17}$$

where $x \equiv \mu\Delta/4$; the starting current is a function of Δ. Minimizing Eq. (17) with respect to Δ yields the minimum starting current, denoted $I_{MIN} \equiv I_{ST}(\Delta_{MIN})$, which is given

by Eq. (17) with

$$x = x_{min} \equiv \frac{1}{2}\left[\frac{n}{\mu} + \left(\frac{n^2}{\mu^2} + 1\right)^{\frac{1}{2}}\right]. \tag{18}$$

The minimum starting current is shown on Fig. 3 by a dashed line labeled I_{MIN}. The gyrotron will not oscillate for currents below this line.

The other starting current shown on Fig. 3 is the line $I = I_{ST}(\Delta_{opt})$, which is labeled $I = I_{START}$. For currents below this line, the beam current is above the starting current at the magnetic field corresponding to the optimum efficiency. This region is referred to as the soft-excitation regime. For currents above the line $I = I_{START}$, the starting current is higher than the beam current, and the device operates in the hard-excitation regime. To operate in this regime, the device must be started in a soft excitation zone and then detuned to the hard excitation zone operating point by changing the current, voltage, magnetic field, or other parameters. Thus the line $I = I_{START}$ delineates the hard and soft excitation regions of the gyrotron, while the line $I = I_{MIN}$ determines the minimum operating current necessary for oscillation.

The gyrotron parameter space defined by F and μ has more than one high efficiency region. Gyrotrons are typically designed and operated with field amplitudes and cavity lengths which correspond to operation in the high efficiency region with the lowest F and μ (e.g. $F \sim 0.1$, $\mu \sim 15 - 20$ in Fig. 2). It is this region for which the technological constraints are most easily satisfied. There are other high efficiency regions in the F-μ parameter space which can have efficiencies comparable to or greater than the peak efficiencies in these usual operating regions. For the fundamental cyclotron interaction, a second high efficiency region is present for $F \sim 0.3$, $\mu \sim 25$. For operation in this second region, the electron beam is bunched by the rf field, and energy is extracted from the bunch. However, before exiting the cavity, the bunch slips in phase enough for the rf field

to begin doing work on the bunch. The bunch then advances in phase to the point where the bunch again does work on the rf field, and the field energy has increased by the time the electrons exit the cavity. This process is analagous to the synchrotron oscillations of the electrons in the ponderomotive potential well of a free electron laser. Such a process is more susceptible to velocity spread and space charge effects. Because of these problems and other technological constraints, it is unclear whether a device could be designed to operate in these additional high efficiency zones. We focus only on the region of F-μ parameter space containing the first high efficiency zone, and all quoted peak efficiencies are for this first high efficiency region. Parts of these additional high efficiency regions are visible on some of the isoefficiency contour plots shown.

The second harmonic isoefficiency F-μ and I-μ contour plots are shown in Figs. 4 and 5, respectively. The Δ_{opt} contours are shown on Fig. 4; the $I = I_{MIN}$ and $I = I_{START}$ lines are shown on Fig. 5. The peak efficiency is $\eta_\perp = 0.72$ and occurs for $F = 0.22$ and $\mu = 16.0$.

The F-μ and I-μ contour plots for the fundamental and second harmonic shown here are in good agreement with those previously calculated by Nusinovich and Erm.[18] They are shown here for completeness. Isoefficiency contour plots for higher harmonics have not been previously presented.

The third harmonic isoefficiency F-μ and I-μ contour plots are shown in Figs. 6 and 7, respectively. The peak efficiency at the third harmonic is $\eta_\perp = 0.57$, which occurs for $F = 0.15$ and $\mu = 16.75$. The fourth harmonic isoefficiency F-μ and I-μ contour plots are shown in Figs. 8 and 9. The peak efficiency at the fourth harmonic occurs at $F = 0.09$ and $\mu = 21.0$ and is $\eta_\perp = 0.45$. The fifth harmonic F-μ and I-μ contour plots are shown in Figs. 10 and 11. The peak efficiency at the fifth harmonic is $\eta_\perp = 0.36$ and occurs at

$F = 0.055$ and $\mu = 26.0$.

A generalized expression for the starting current as a function of the detuning parameter Δ can be derived from equations (17) and (18). The ratio of $I_{ST}(\Delta)$ and the minimum starting current I_{MIN} can be written as

$$\frac{I_{ST}(\Delta)}{I_{MIN}} = \left[\frac{1-\frac{n}{\mu x}}{\frac{\Delta}{\Delta_{MIN}}-\frac{n}{\mu x}}\right] \exp\left[2x^2\left(\frac{\Delta^2}{\Delta_{MIN}^2}-1\right)\right], \tag{19}$$

where x is given by equation (18) and $\Delta_{MIN} = 4x/\mu$. For $n/\mu \ll 1$, which is almost always valid for harmonic gyrotrons, equation (19) simplifies to

$$\frac{I_{ST}(\Delta)}{I_{MIN}} = \left(\frac{\Delta}{\Delta_{MIN}}\right)^{-1} \exp\left[\frac{1}{2}\left(\frac{\Delta^2}{\Delta_{MIN}^2}-1\right)\right]. \tag{20}$$

This simple expression for the starting current has no explicit dependence on harmonic number or cavity length (μ); the normalized I_{ST} depends only on the single magnetic field parameter Δ. Equation (20) is plotted in Fig. 12.

Calculations have also been performed for the case where the longitudinal rf field profile is an asymmetric gaussian. It is well known that the gyrotron efficiency is strongly dependent on the axial field profile. Although complicated axial field profiles can yield very high efficiencies,[4] it is often difficult to realize them in practice. One class of axial field profiles which are not physically unrealistic and can be easily modeled are those of an asymmetric gaussian. An asymmetric gaussian field profile with asymmetry parameter A can be defined by

$$f(z) = \begin{cases} \exp\left[-\left[\frac{(A+1)z}{AL}\right]^2\right] & \text{for } z < 0; \\ \exp\left[-\left[\frac{(A+1)z}{L}\right]^2\right] & \text{for } z \geq 0. \end{cases}$$

For $A = 1$, the symmetric gaussian of equation (15) is recovered. For $A > 1$ the field profile is that of an asymmetric gaussian for which the peak of the rf field is shifted towards the

output end ($z > 0$) of the cavity. This profile has the same stored energy and e^{-1} width for $A \neq 1$ as does the symmetric gaussian, so the definition of the current parameter is unchanged.

The presence of even a moderate asymmetry in the axial field profile can substantially increase both the maximum efficiency and the efficiency at other operating points corresponding to non-optimum parameters. The F-μ isoefficiency contour plot for the second harmonic and an asymmetry parameter of $A = 2$ is shown in Fig. 13. Such a field profile is not unrealistic for moderate and high diffractive Q gyrotron cavities. The use of an asymmetric gaussian field profile for the design of harmonic gyrotrons would allow lower wall loadings (lower F) than would a symmetric gaussian at the same efficiency [23].

The results presented can also be applied to gyrotrons with open, Fabry-Perot type resonators with a suitable redefinition of parameters. Operation at the fundamental in such a resonator has been considered by Sprangle *et al.* [25]; operation at harmonics has been considered by Levush and Manheimer[26]. For a thin pencil beam propagating at a right angle to the optical axis of the quasioptical Fabry-Perot resonator, the equations of motion may be written as [27]

$$\frac{du}{d\varsigma} = 2F \cos\left(ky_g - \frac{n\pi}{2}\right) f(\varsigma)\,(1-u)^{\frac{n}{2}} \sin\theta$$

$$\frac{d\theta}{d\varsigma} = \Delta - u - nF \cos\left(ky_g - \frac{n\pi}{2}\right) f(\varsigma)\,(1-u)^{\frac{n}{2}-1} \cos\theta$$

where $k = 2\pi/\lambda$ and y_g is the electron guiding center coordinate along the resonator axis. The field distribution function $f(\varsigma)$ is a gaussian given by $f(\varsigma) = \exp[-(2\varsigma/\mu)^2]$; this corresponds to the transverse profile of a TEM_{00} gaussian beam. The dimensionless parameters F, I, and μ, are defined as follows for the quasioptical gyrotron,

$$\mu \equiv \frac{\beta_{\perp o}^2}{\beta_{\parallel o}} \left(\frac{2\pi w_o}{\lambda}\right)$$

$$F \equiv \frac{E_0 \beta_{\perp 0}^{n-4}}{B_0} \left(\frac{n^{n-1}}{2^{n-1} n!} \right)$$

$$I \equiv 1.514 \times 10^{-5} \frac{Q_T I_A}{\gamma_0} \beta_{\perp 0}^{2(n-3)} \left(\frac{\lambda}{d} \right) \left(\frac{\lambda}{w_o} \right)^2 \left(\frac{n^n}{2^n n!} \right)^2 .$$

The magnetic field parameter Δ is unchanged. The TEM_{00} gaussian beam e^{-1} radius is w_o, and d is the separation of the mirrors which form the quasioptical cavity. The results presented in Figures 2-12 are immediately applicable to the case of a quasioptical gyrotron with a pencil electron beam (ky_g = constant). For an annular electron beam, where $y_g = R_e \sin\varphi$ with $\varphi \in [0, 2\pi)$, an additional average over the electron guiding centers y_g is required to obtain the efficiency of a quasioptical gyrotron.

The above results for a circular symmetric cavity with a rotating rf field and a Fabry-Perot cavity with a pencil beam can be extended to other field and cavity configurations. Luchinin and Nusinovich have presented an analytic theory which relates the orbital efficiency as calculated above to the efficiency of gyrotrons with other geometrical configurations[28]. The above results are thus applicable to other configurations, such as that of a circular cavity with disturbed axial symmetry (e.g. slots) or a Fabry-Perot cavity with an annular electron beam. Consequently, these nonlinear results allow the optimization of the design of harmonic gyrotrons with many different geometries.

IV. DISCUSSION

The general nonlinear results presented here have application to the design and analysis of harmonic gyrotrons. Because the efficiency and optimum magnetic detuning have been calculated as functions of generalized parameters, the results are valid for a wide range of operating conditions. In particular. provided the condition in equation (12) is satisfied, the results are valid for arbitrary cavity mode, voltage, current, beam radius, electron pitch factor, and cavity length.

As an example of the application of this nonlinear theory to an actual harmonic gyrotron experiment, we consider the second harmonic generation of 25 kW of rf power at 241.02 GHz in the $TE_{11,2,1}$ mode.[13] For this experiment, the electron beam parameters were $\beta_{\perp 0}/\beta_{\parallel 0} = 1.5$, $V_b = 64.3\,\mathrm{kV}$, $I_A = 6\,\mathrm{A}$, and $R_e = 1.82\,\mathrm{mm}$. The rf longitudinal field profile was calculated from a computer code[29] and fitted with a gaussian. The width of the gaussian determines L in the definition of μ. For this experiment, $L = 1.26$ cm, $\mu = 18.2$, and the diffractive and ohmic Q are 4800 and 15770, respectively. The current parameter is $I = 6.35 \times 10^{-3}$ for a current of 6 A. From Figure 5, the transverse efficiency is $\eta_\perp = 0.43$, and the total efficiency is thus $\eta_T = 0.23$. The discrepancy between the theoretical and experimental efficiency is probably due to a lower ohmic Q, higher diffractive Q due to an improperly matched window, or beam velocity spread.[13]

The value of presenting the efficiency in terms of normalized parameters lies not only in the wide applicability of the results to experimental conditions, but also the resulting ability to achieve optimized gyrotron designs. Ohmic heating of the walls, voltage depression of the beam. beam thickness, and space charge effects all result in design constraints which can be expressed in terms of the same generalized parameters [23]. The combination of these constraints and the isoefficiency contour plots allows a straightforward optimization of the

design of harmonic gyrotrons.

The problem of mode competition and multimode oscillation has not been discussed here. Operation at harmonics of the cyclotron frequency can be hampered by mode competition from the fundamental and lower harmonics of ω_c [30,31]. However, careful choice of operating mode, cavity design, and beam placement can allow high efficiency single mode operation at harmonics of the cyclotron frequency.

V. CONCLUSIONS

Numerical results have been presented for the nonlinear efficiency of gyrotron operation for the fundamental and second through fifth harmonics of the cyclotron frequency. Efficiencies as high as 0.72, 0.57, 0.45, and 0.36 are reported for the second, third, fourth, and fifth cyclotron harmonics, respectively.

The effect of asymmetric longitudinal field profiles has been demonstrated, and the second harmonic efficiency has been presented for an asymmetric gaussian field profile with asymmetry parameter $A = 2$. Such field profiles should be physically realizable in actual cavity designs. Presentation of the nonlinear efficiency in terms of general normalized parameters allows both the calculation of the efficiency for non-optimum parameters such as may occur in experiments and the optimization of the design of harmonic gyrotrons. The existence of moderate efficiencies even for the higher $(3\omega_c - 5\omega_c)$ harmonics substantiates arguments for the development of high frequency (millimeter and submillimeter wave) gyrotrons by operation at harmonics. Alternatively, for lower microwave frequencies, operation at harmonics could allow the use of very low magnetic fields.

ACKNOWLEDGEMENTS

The authors wish to thank K.E.Kreischer and T.M.Tran for many helpful discussions. This work was supported by the U.S. Department of Energy Contract No. DE-AC02-78ET51013.

REFERENCES

[1] J.L.Hirshfield and V.L.Granatstein, IEEE Trans. Microwave Theory Tech., **MTT-25**, 522 (1977).

[2] V.A.Flyagin, A.V.Gaponov, M.I.Petelin, and V.K.Yulpatov, IEEE Trans. Microwave Theory Tech., **MTT-25**, 514 (1977).

[3] R.S.Symons and H.R.Jory, in Advances in Electronics and Electron Physics, Vol.55 (Academic Press, New York, 1981).

[4] A.V.Gaponov, V.A.Flyagin, A.L.Goldenberg, G.S.Nusinovich, Sh.E.Tsimring, V.G. Usov, and S.N.Vlasov, Int. J. Electron., **51**, 277 (1981).

[5] H. Hsuan, K. Bol, N. Bowen, D. Boyd, A. Cavallo, A. Dimits, J. Doane, G. Elder, M. Goldman, B. Grek, C. Hoot, D. Johnson, A. Kritz, B. Leblanc, P. Manintveld, R. Polman, S. Sesnic, H. Takashashi, and F. Tenney, Proc. Fourth Int. Symp. on Heating in Toroidal Plasmas, Rome, 1984, pp. 809-833.

[6] R.Prater, S.Ejima, S.H.Lin, C.Moeller, H.Y.Hsu, K.Matsuda, and R.Stockdale, Proc. Fourth Int. Symp. on Heating in Toroidal Plasmas, Rome, 1984

[7] V. V. Alikaev, *et al.*, *Sov. J. Plasma Phys.*, **9**, 196 (1983).

[8] P.Woskoboinikow, D.R.Cohn, and R.J.Temkin, Int. J. Infrared and Millimeter Waves, **4**, 205 (1983).

[9] A.Sh.Fiks, V.A.Flyagin, A.G.Luchinin, G.S.Nusinovich, and B.V.Shishkin, Proc. Fourth Int. Symp. on Heating in Toroidal Plasmas, Rome, Italy (1984).

[10] N.I.Zaytsev, T.B.Pankratova, M.I.Petelin, and V.A.Flyagin, Radio Eng. Electron. Phys., **19**, 103 (1974).

[11] J.D.Silverstein, R.M.Curnutt, and M.E.Read, Int. J. Electron., **53**, 539 (1982).

[12] B.G.Danly, W.J.Mulligan, R.J.Temkin, and T.C.L.G.Sollner, Appl.Phys.Lett., **46**, 728 (1985).

[13] J.L.Byerly, B.G.Danly, K.E.Kreischer, R.J.Temkin, W.J.Mulligan, and P.Woskoboinikow, Int. J. Electron. **57**, 1033 (1984).

[14] H.Guo, Z.Chen, S.Zhang, and D.Wu, Int. J. Electron., **51**, 485 (1981).

[15] P.Boulanger, P.Charbit, G.Faillon, E.Kammerer, and G.Mourier, Int. J. Electron, **53**, 523 (1982).

[16] K.R.Chu, Phys. Fluids, **21**, 2354 (1978).

[17] H.Uhm, R.C.Davidson, K.R.Chu, Phys. Fluids, **21**, 1877 (1978).

[18] G.S. Nusinovich, and R.E. Erm, Elektronnaya Tekhnika, Ser. 1, Elektronika SVCh, 55 (1972).

[19] A.W.Fliflet, M.E.Read, K.R.Chu, and R.Seeley, Int. J. Electron., **53**, 505 (1982).

[20] V.L.Bratman, N.S.Ginzburg, G.S.Nusinovich, M.I.Petelin, and P.S.Strelkov, Int. J. Electron., **51**, 541 (1981).

[21] K.R.Chu and J.L.Hirshfield, Phys. Fluids, **21**, 461 (1978).

[22] M.K.Haldar and A.H.Beck, Electron. Lett., **15**, 487 (1979).

[23] K.E.Kreischer, B.G.Danly, J.B.Schutkeker, and R.J.Temkin, submitted to IEEE J. Plasma Science, (1985).

[24] K.E.Kreischer and R.J.Temkin, Int. J. Infrared and Millimeter Waves, **1**, 195, (1980).

[25] P.Sprangle, J.L.Vomvoridis, and W.M.Manheimer, Phys. Rev. A, **23**, 3127 (1981).

[26] B.Levush, A.Bondeson, W.M.Manheimer, and E.Ott. Int. J. Electron., **54**, 749 (1983).

[27] T.M.Tran, B.G.Danly, K.E.Kreischer, J.B.Schutkeker, and R.J.Temkin, submitted to Phys. Fluids, (1985).

[28] A.G.Luchinin and G.S.Nusinovich, Int. J. Electron., **57**, 827 (1984).

[29] A.W.Fliflet and M.E.Read, Int. J. Electron., **51**, 475 (1981).

[30] G.S.Nusinovich, Int. J. Electron., **51**, 457 (1981).

[31] V.E.Zapevalov, G.S.Korablev, and Sh.Ye.Tsymring, Radio Eng. Electron. Phys., **22**, 1661 (1977).

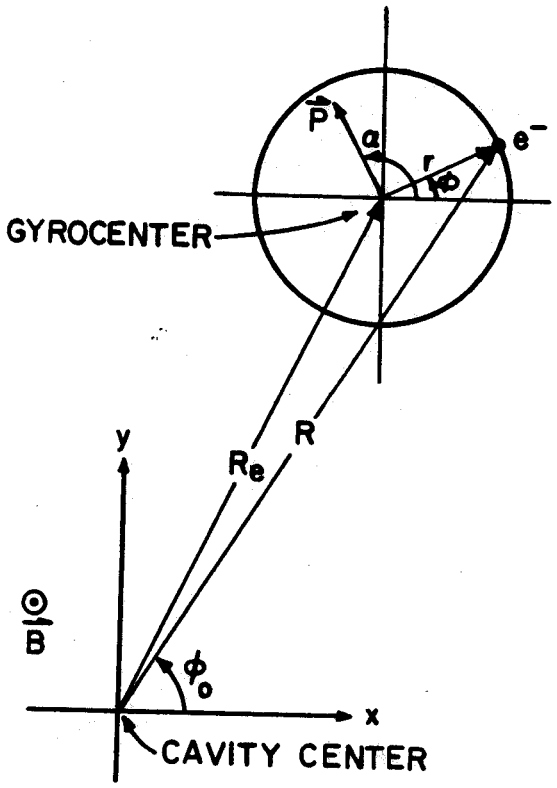

Fig.1

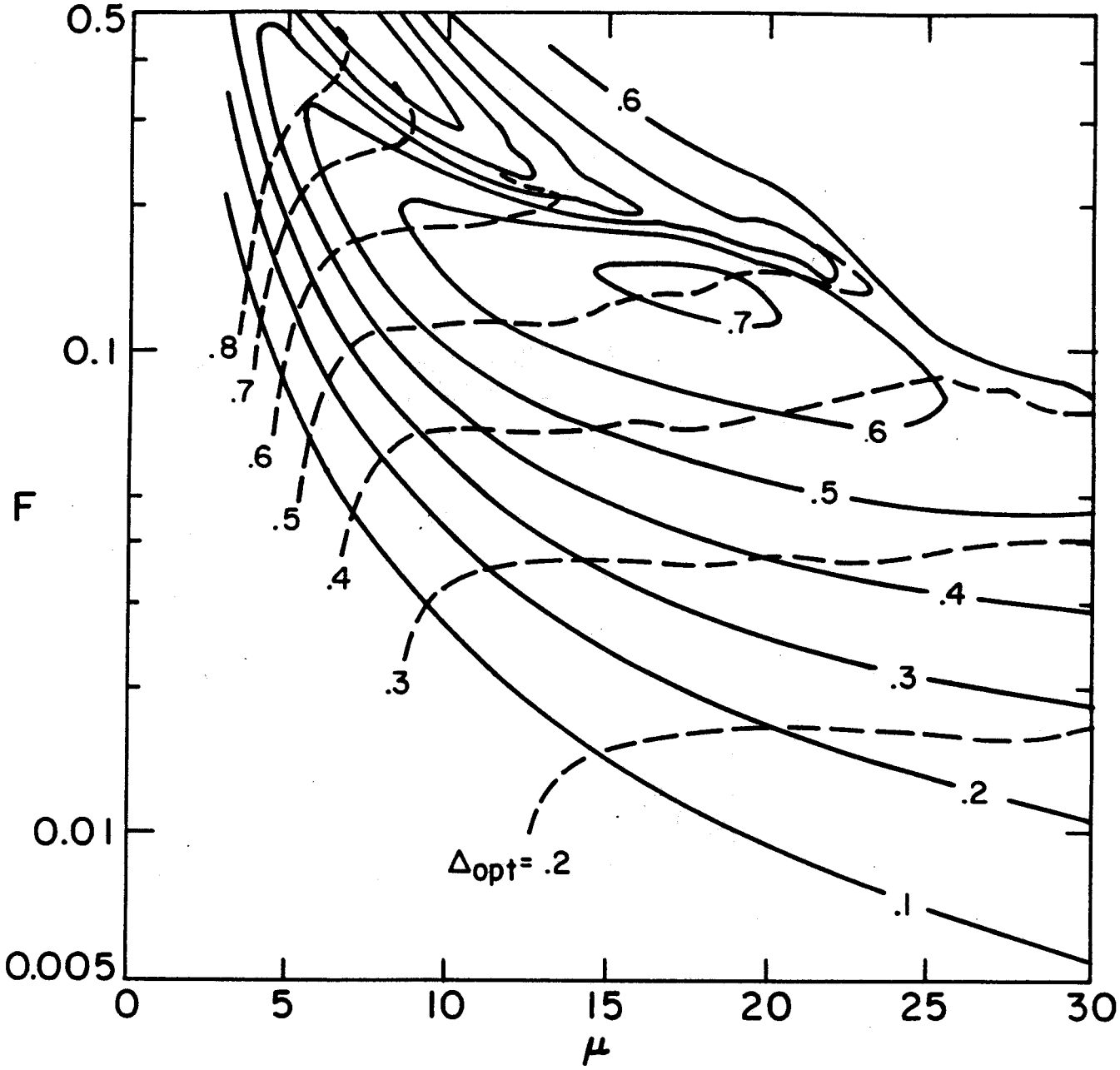

Fig.2

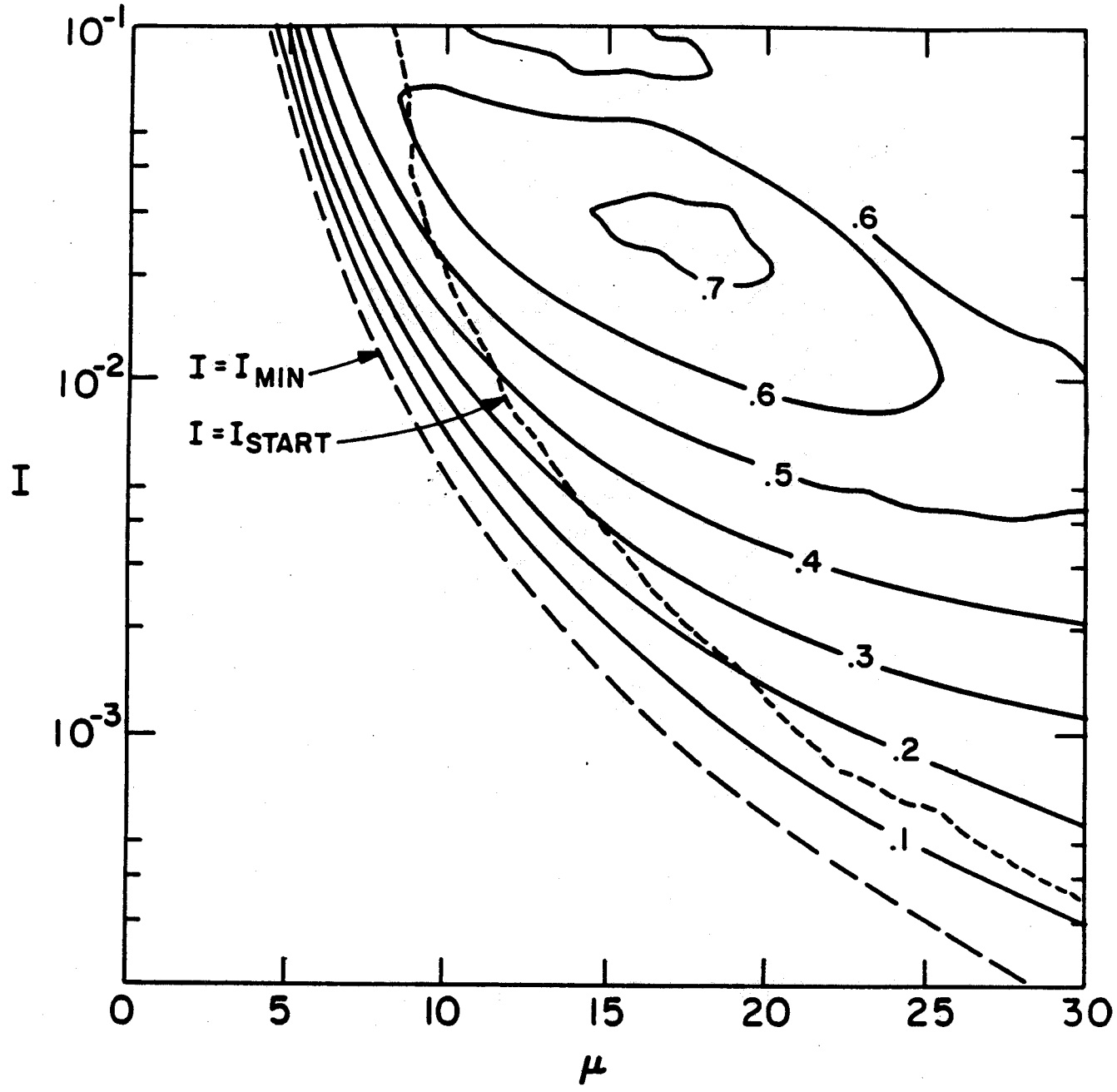

Fig.3

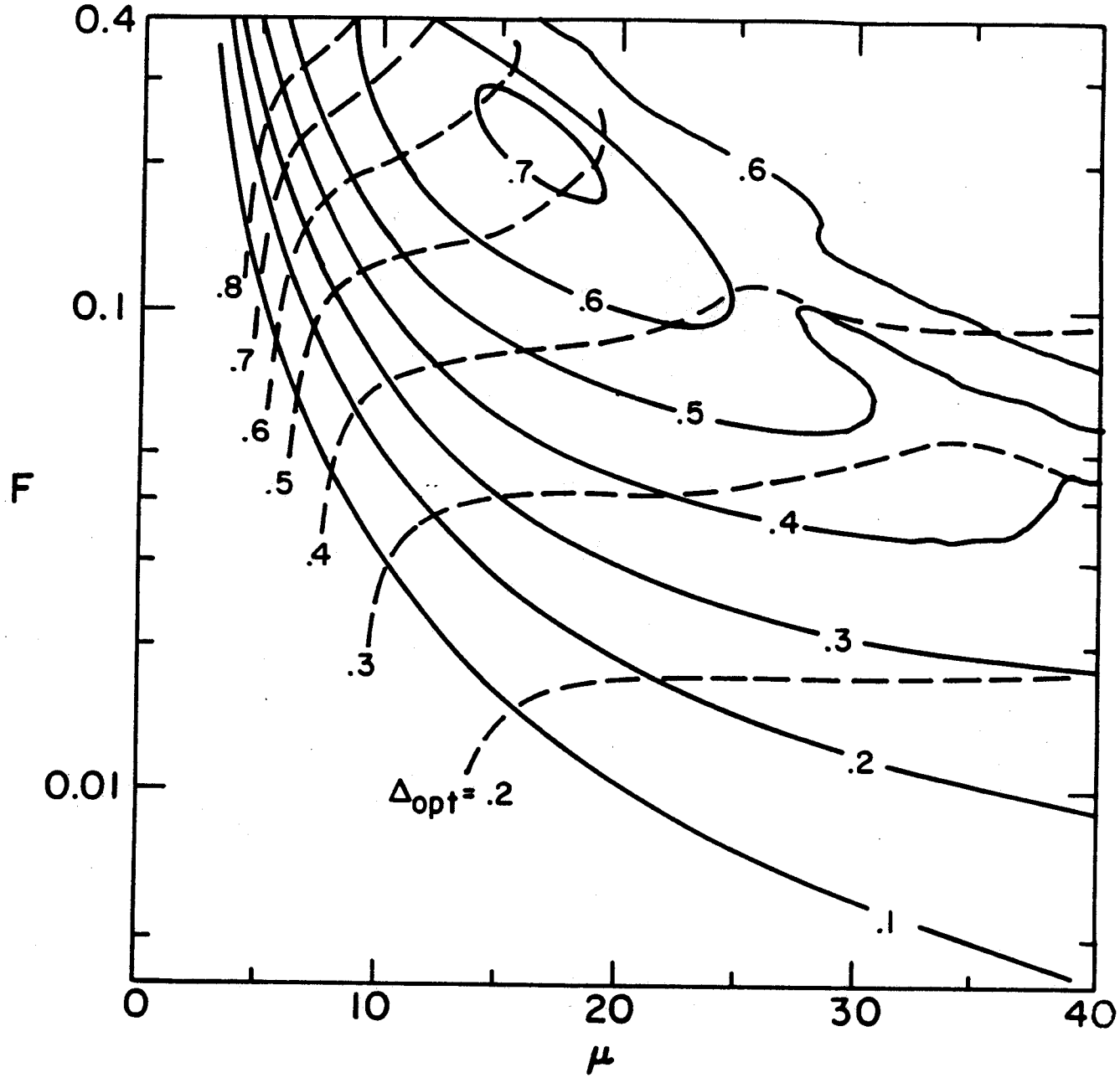

Fig.4

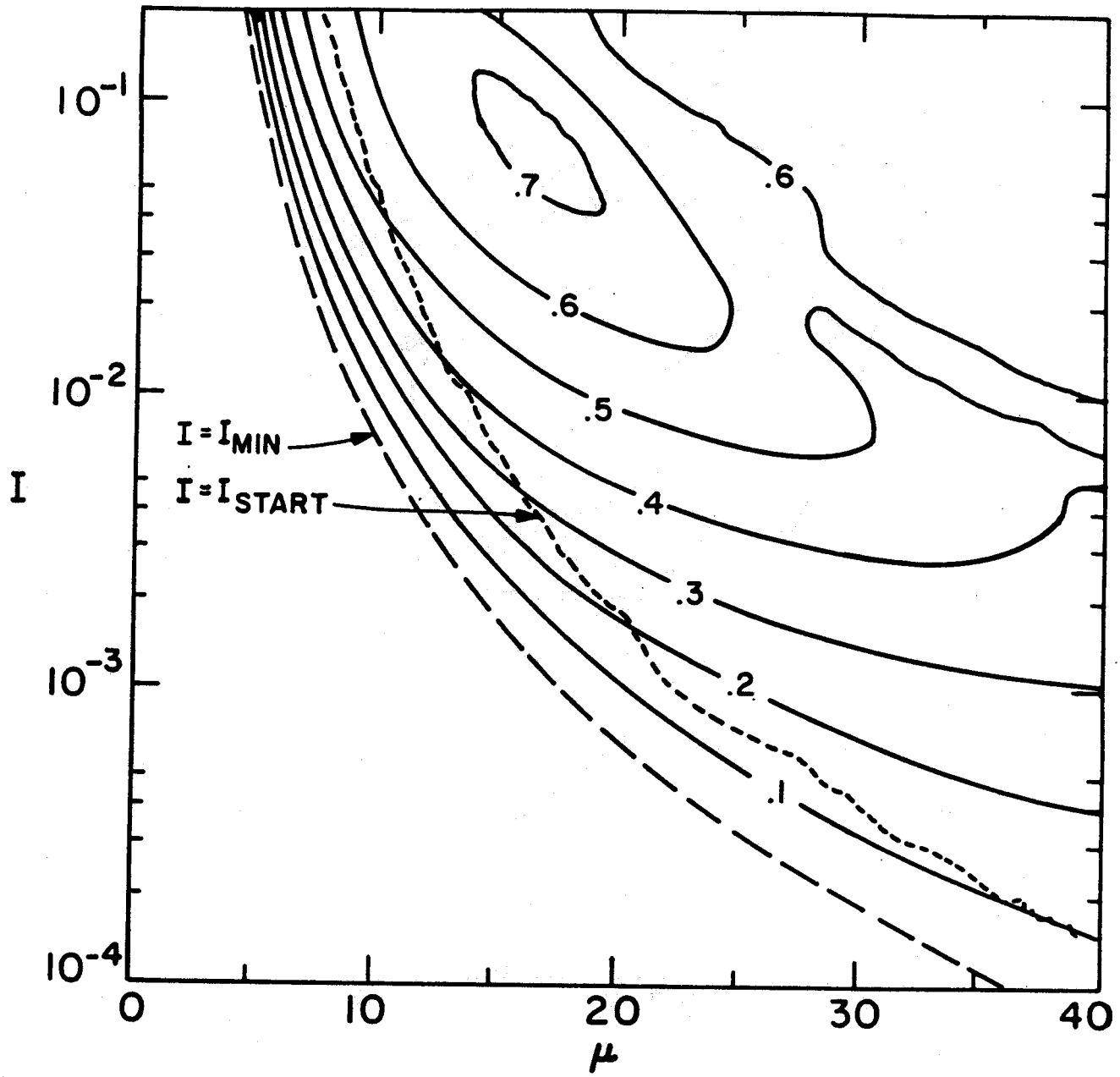

Fig.5

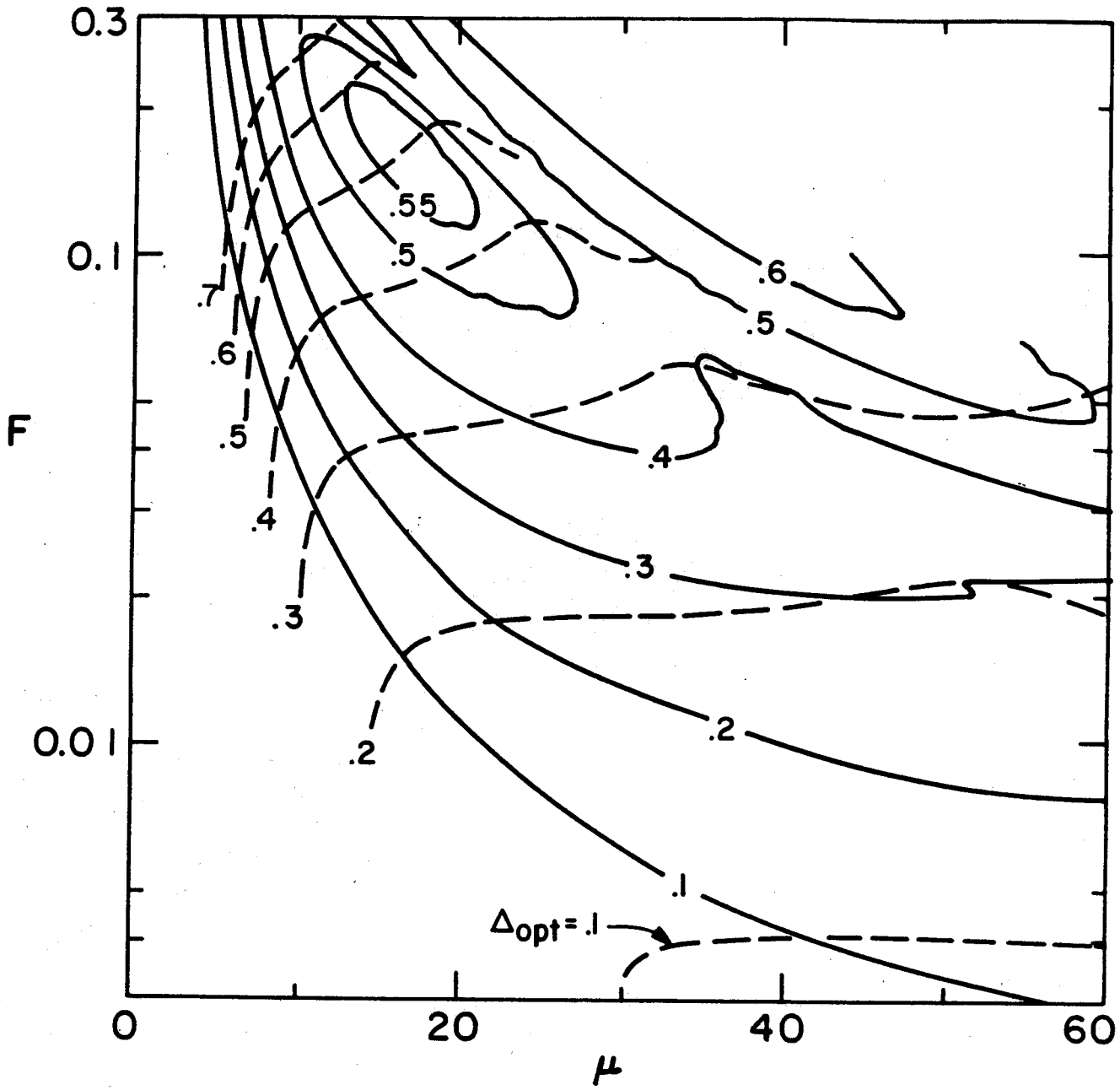

Fig.6

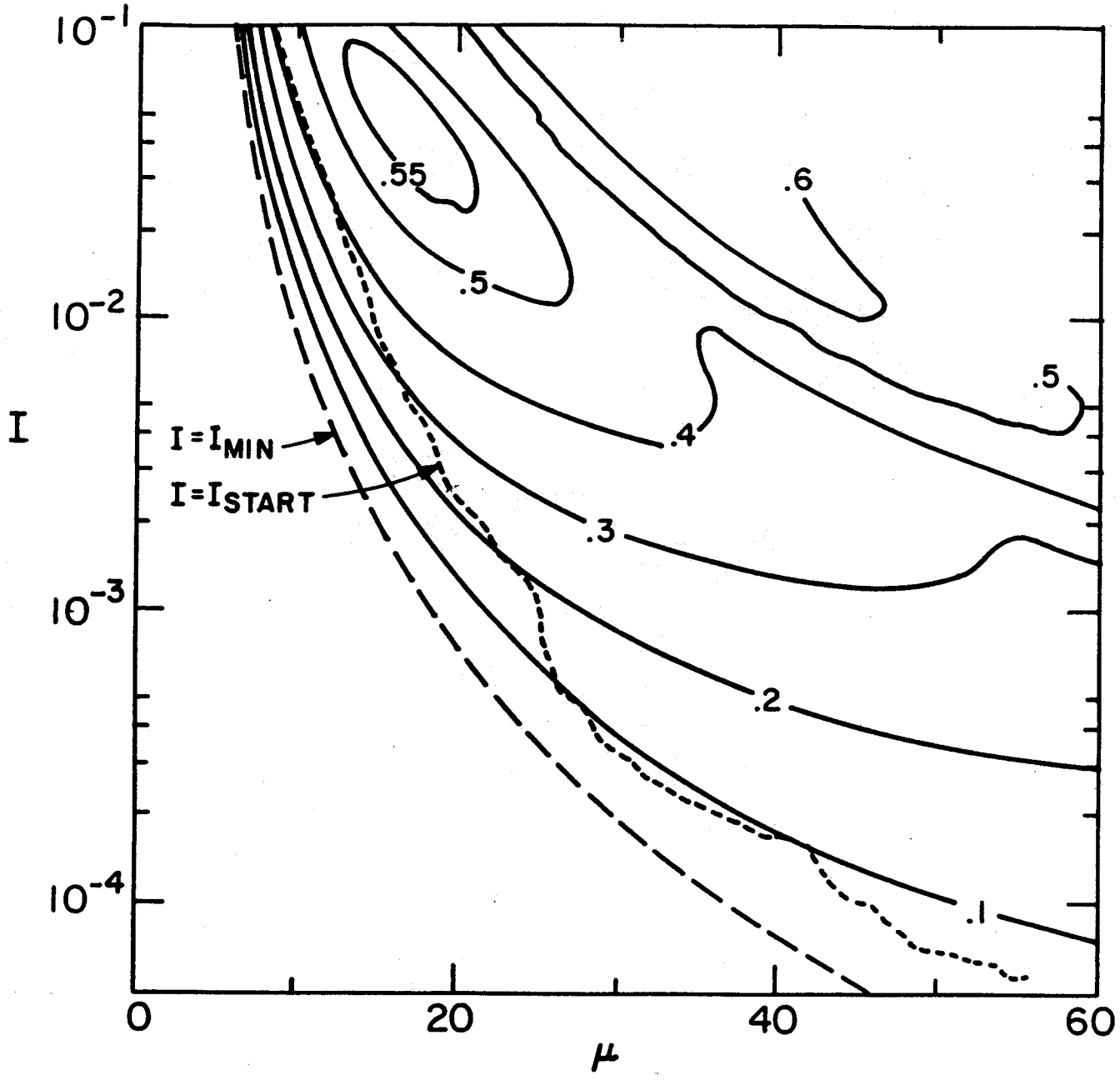

Fig.7

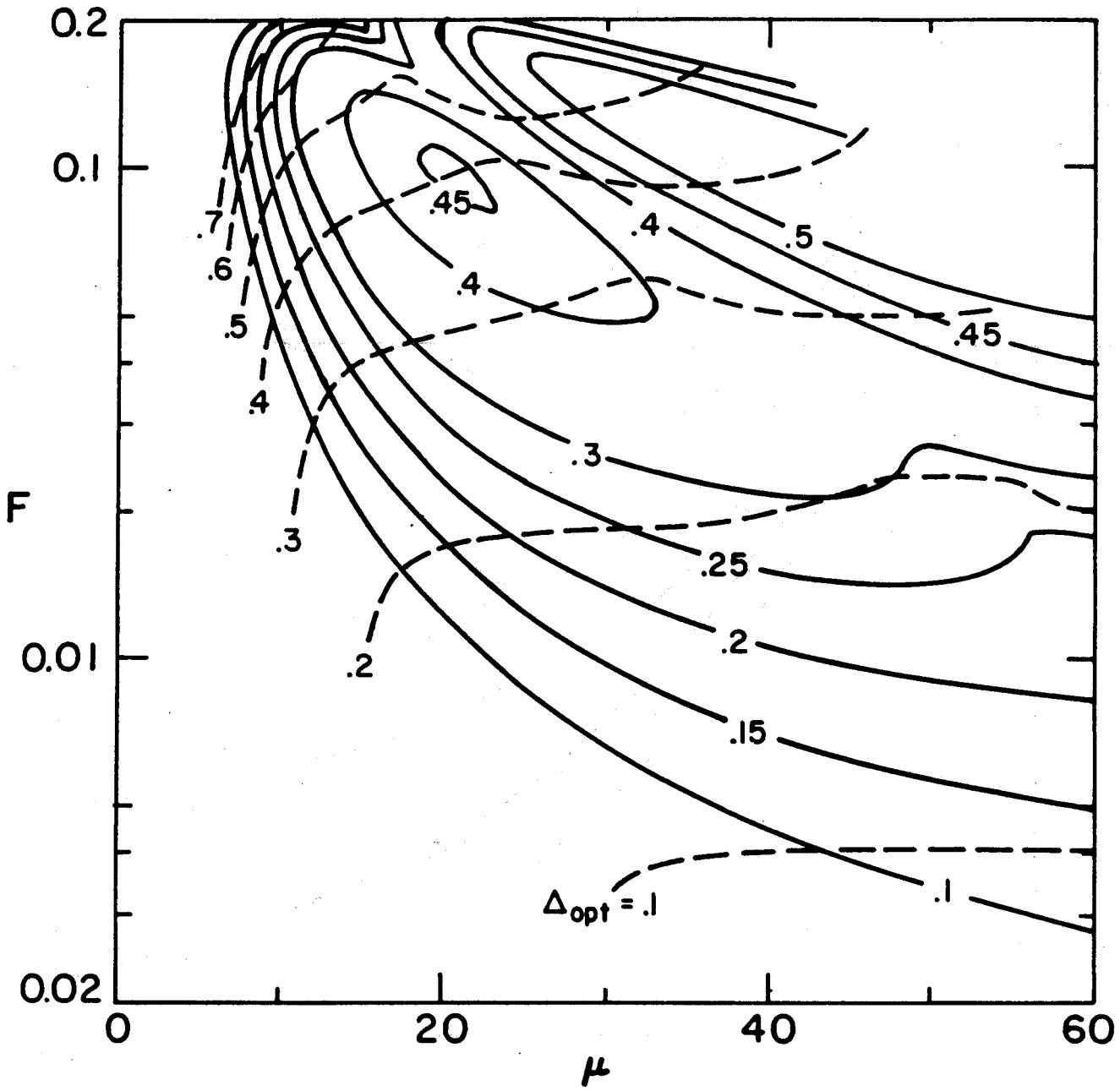

Fig.8

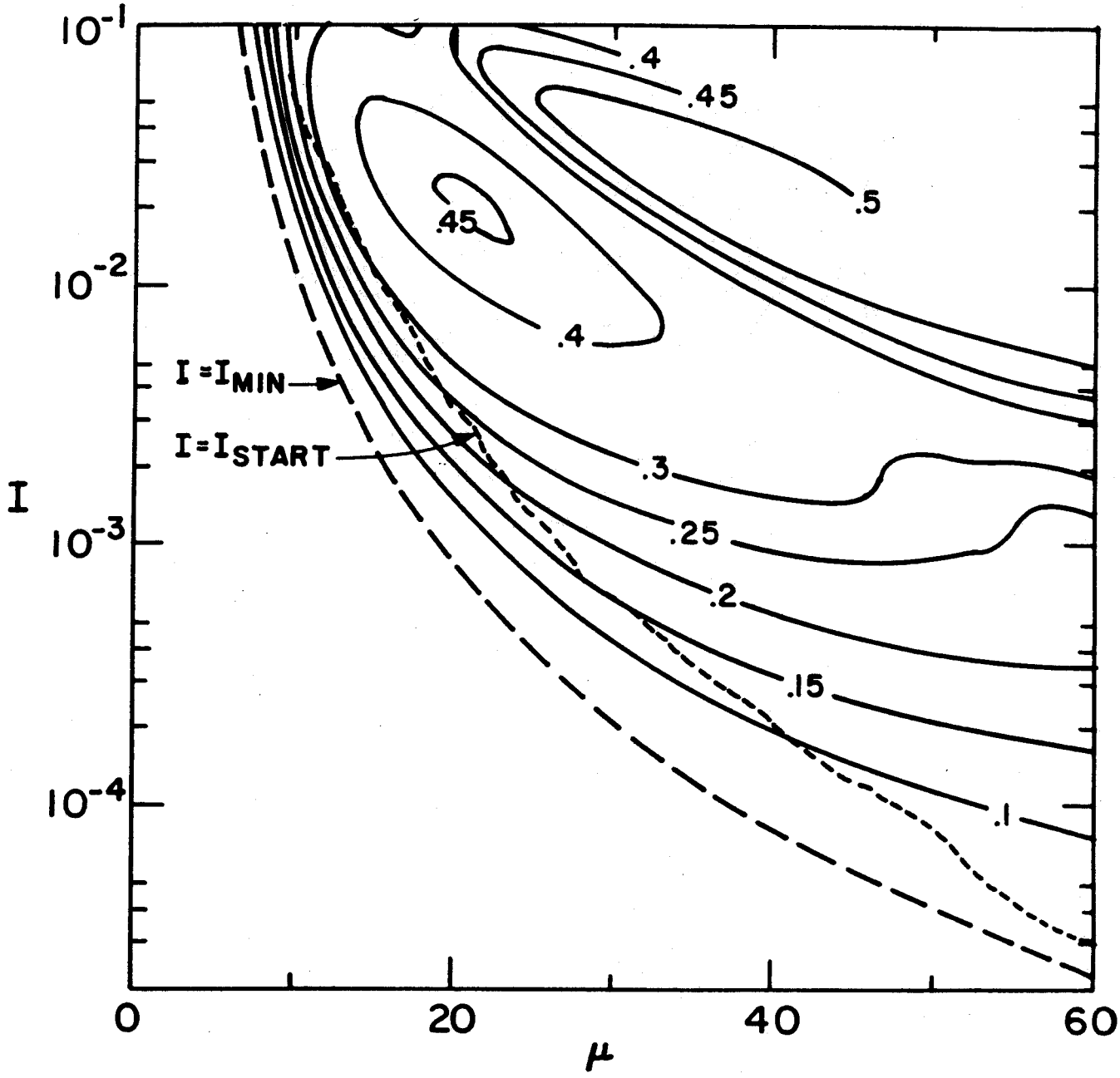

Fig.9

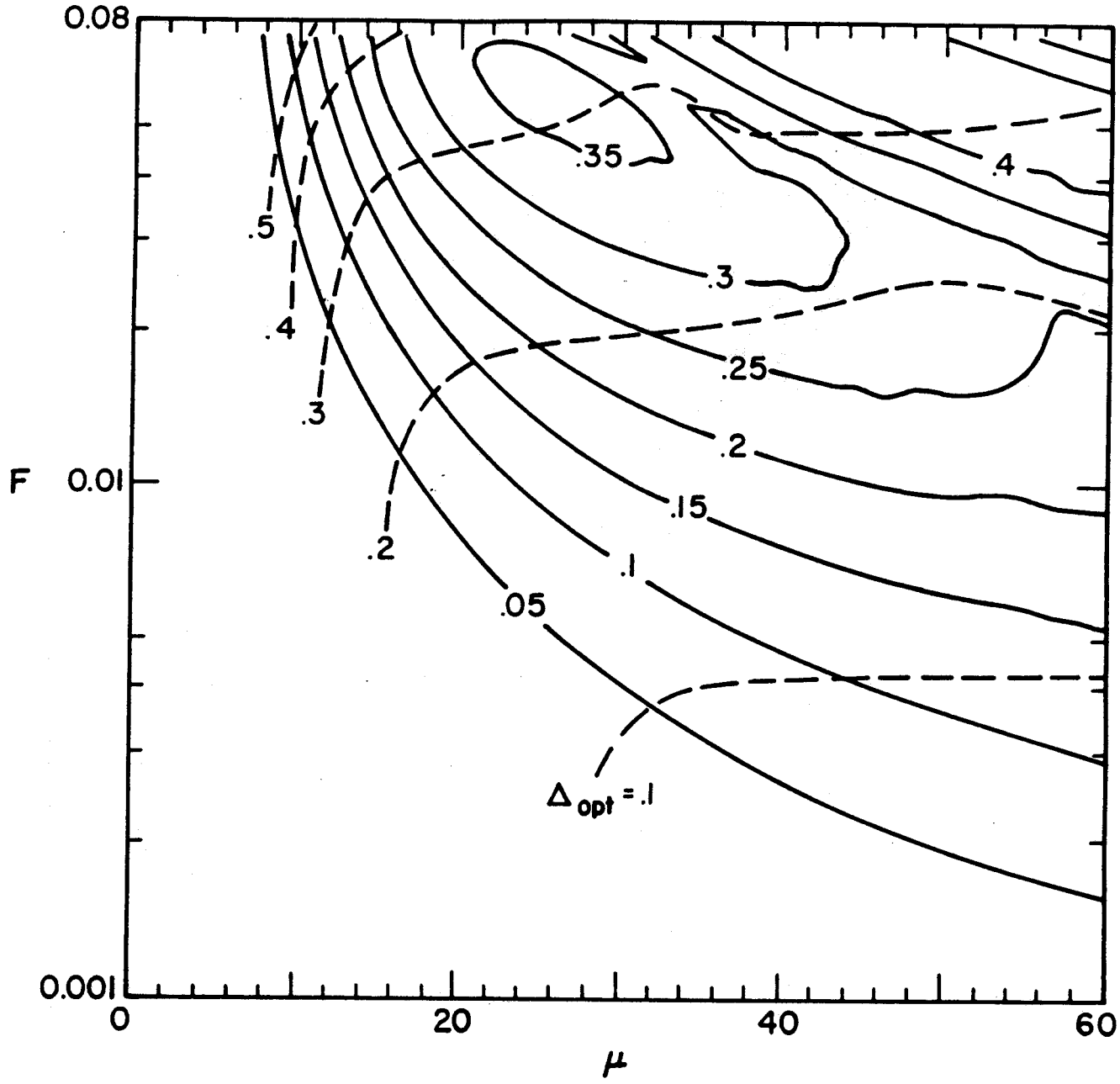

Fig.10

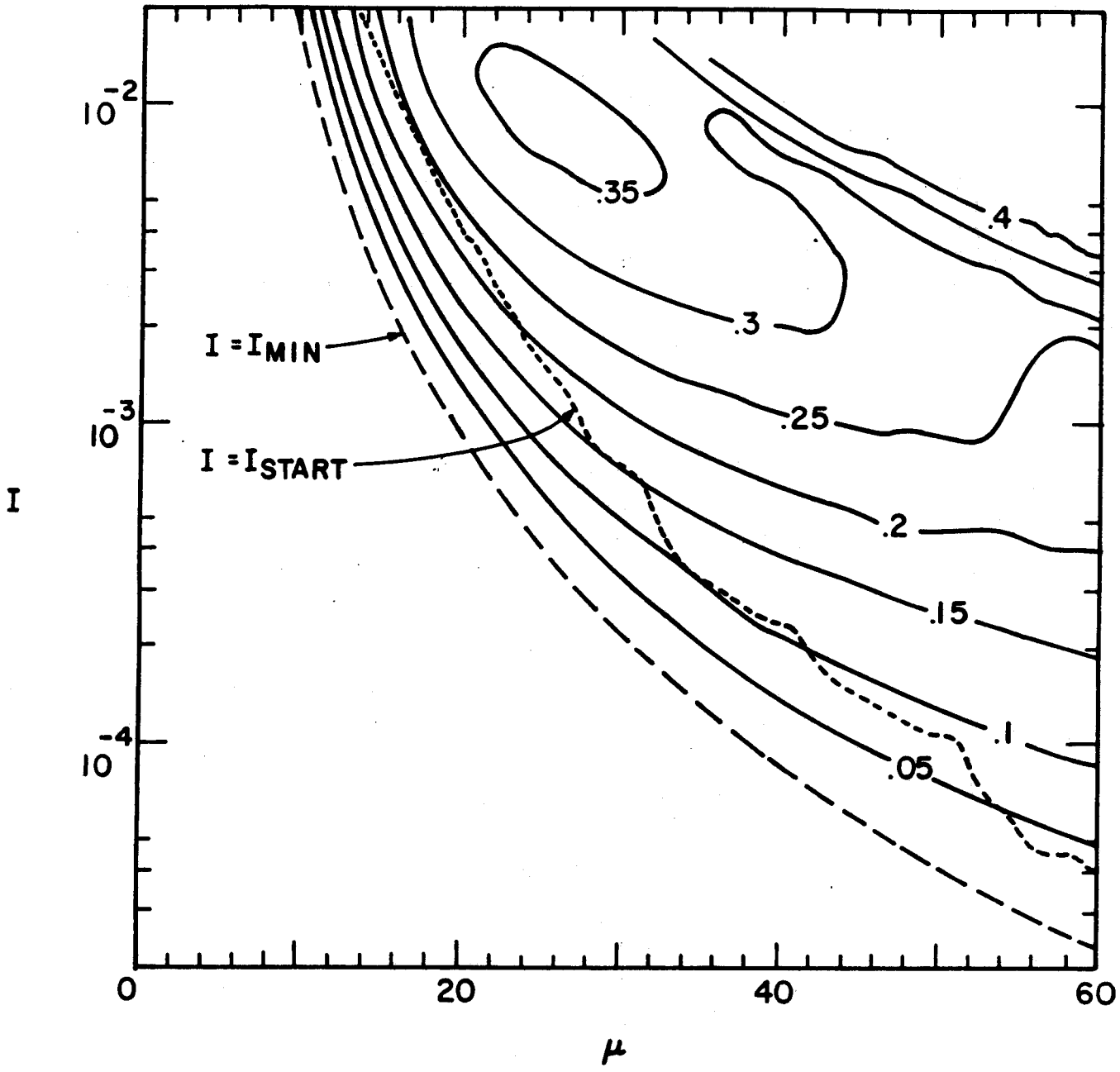

Fig.11

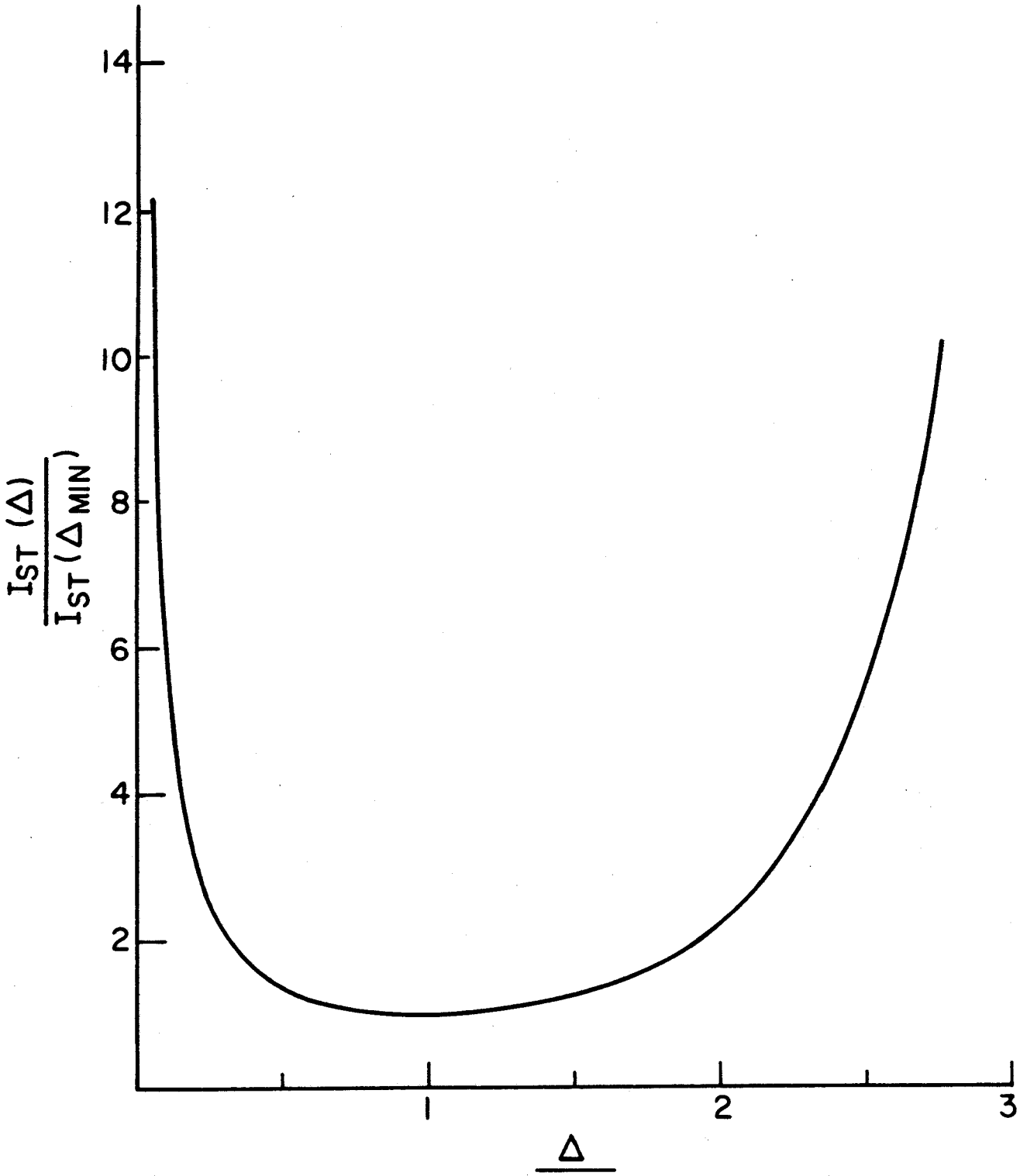
14
12
10
8
6
4
2
1
2
3
$\frac{I_{ST}(\Delta)}{I_{ST}(\Delta_{MIN})}$
$\frac{\Delta}{\Delta_{MIN}}$

Fig.12

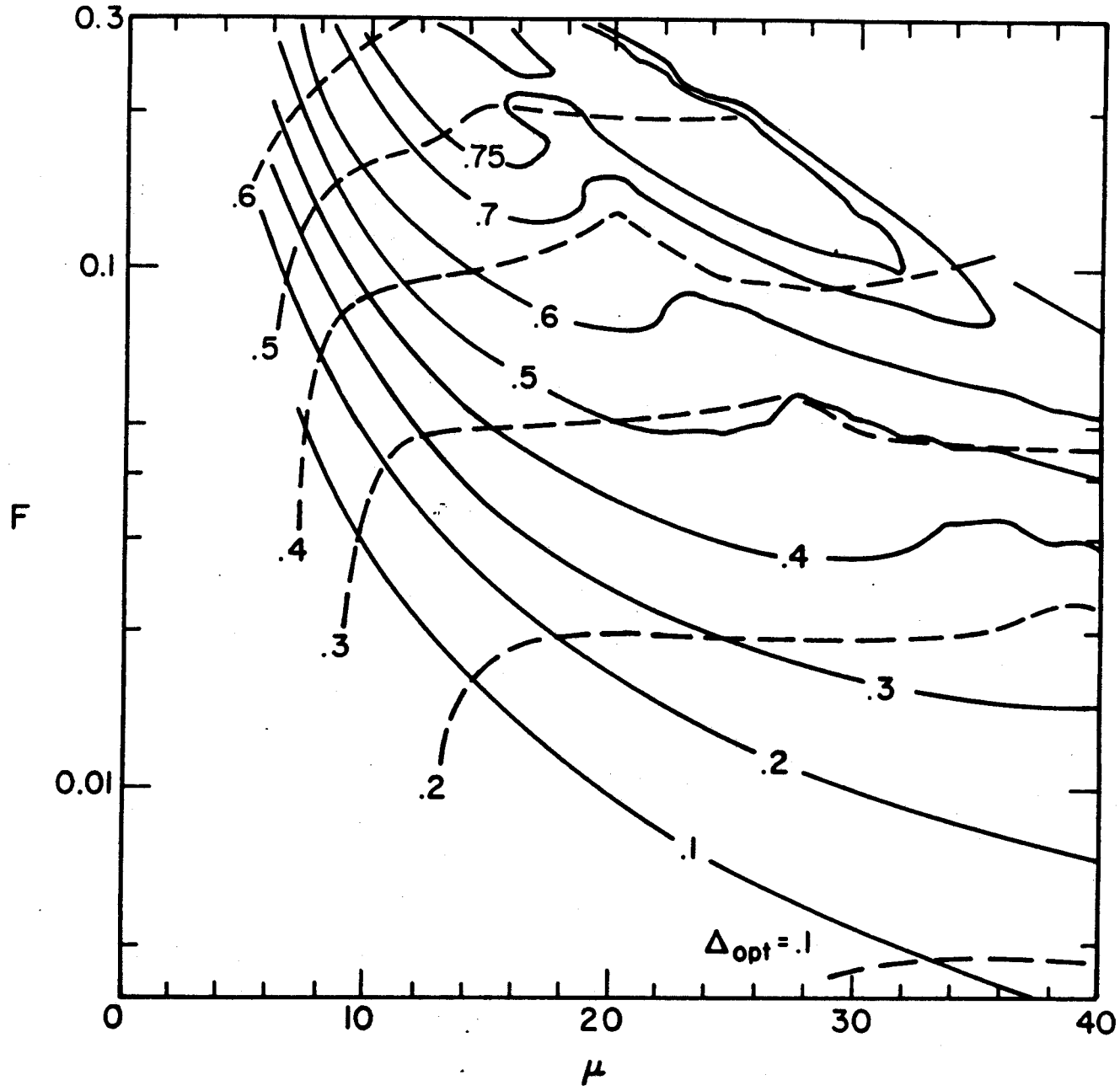

Fig.13

FIGURE CAPTIONS

Fig. 1 Coordinate system and definition of variables for analysis of harmonic gyrotron.

Fig. 2 Contour plot of transverse efficiency $\eta_\perp$ (solid lines) and optimum magnetic field Δ_{opt} (dashed lines) as a function of field amplitude F and cavity length μ for fundamental cyclotron interaction ($\omega \approx \omega_c$).

Fig. 3 Contour plot of transverse efficiency $\eta_\perp$ (solid lines) as a function of normalized beam current I and cavity length μ for fundamental ($\omega \approx \omega_c$) cyclotron interaction. The $I = I_{MIN}$ and $I = I_{START}(\Delta_{opt})$ lines are shown.

Fig. 4 Contour plot of transverse efficiency $\eta_\perp$ (solid lines) and optimum magnetic field Δ_{opt} (dashed lines) as a function of field amplitude F and cavity length μ for the second harmonic cyclotron interaction ($\omega \approx 2\omega_c$).

Fig. 5 Contour plot of transverse efficiency $\eta_\perp$ (solid lines) as a function of normalized beam current I and cavity length μ for the second harmonic ($\omega \approx 2\omega_c$) cyclotron interaction. The $I = I_{MIN}$ and $I = I_{START}(\Delta_{opt})$ lines are shown.

Fig. 6 Contour plot of transverse efficiency $\eta_\perp$ (solid lines) and optimum magnetic field Δ_{opt} (dashed lines) as a function of field amplitude F and cavity length μ for the third harmonic cyclotron interaction ($\omega \approx 3\omega_c$).

Fig. 7 Contour plot of transverse efficiency $\eta_\perp$ (solid lines) as a function of normalized beam current I and cavity length μ for the third harmonic ($\omega \approx 3\omega_c$) cyclotron interaction. The $I = I_{MIN}$ and $I = I_{START}(\Delta_{opt})$ lines are shown.

Fig. 8 Contour plot of transverse efficiency $\eta_\perp$ (solid lines) and optimum magnetic field Δ_{opt} (dashed lines) as a function of field amplitude F and cavity length μ for the fourth harmonic cyclotron interaction ($\omega \approx 4\omega_c$).

Fig. 9 Contour plot of transverse efficiency $\eta_\perp$ (solid lines) as a function of normalized beam current I and cavity length μ for the fourth harmonic ($\omega \approx 4\omega_c$) cyclotron interaction. The $I = I_{MIN}$ and $I = I_{START}(\Delta_{opt})$ lines are shown.

Fig. 10 Contour plot of transverse efficiency $\eta_\perp$ (solid lines) and optimum magnetic field Δ_{opt} (dashed lines) as a function of field amplitude F and cavity length μ for the fifth harmonic cyclotron interaction ($\omega \approx 5\omega_c$).

Fig. 11 Contour plot of transverse efficiency $\eta_\perp$ (solid lines) as a function of normalized beam current I and cavity length μ for the fifth harmonic ($\omega \approx 5\omega_c$) cyclotron interaction. The $I = I_{MIN}$ and $I = I_{START}(\Delta_{opt})$ lines are shown.

Fig. 12 Generalized starting current as a function of relative magnetic field.

Fig. 13 Contour plot of transverse efficiency $\eta_\perp$ (solid lines) and optimum magnetic field Δ_{opt} (dashed lines) as a function of field amplitude F and cavity length μ for the second harmonic and an asymmetric field profile with $A = 2$.